Complex Patterns in a Periodically Forced Surface Reaction

Matthias Bertram, Carsten Beta, Harm H. Rotermund,* and Gerhard Ertl

Fritz-Haber-Institut der Max-Planck-Gesellschaft, Faradayweg 4-6, 14195 Berlin, Germany

Received: January 23, 2003; In Final Form: June 6, 2003

Effects of time-periodic, spatially uniform forcing on oscillatory chemical turbulence are studied in experiments with catalytic CO oxidation on a platinum(110) single-crystal surface. A variety of complex spatiotemporal reaction−diffusion patterns is investigated under variation of the forcing amplitude and frequency. Near harmonic resonance with the forcing, intermittent turbulence characterized by the presence of localized turbulent bubbles on a homogeneously oscillating background and disordered cellular structures are observed. In the parameter region where the system exhibits 2:1 subharmonic resonance, irregular oscillatory stripes and cluster patterns are found. For such resonant patterns, a frequency demodulation technique is used to reconstruct phase and amplitude variables from the experimental data.

1. Introduction

Periodic forcing (e.g., tidal current, circadian rhythm, beating of the heart) is abundantly present in nature. When a nonlinear oscillator periodically oscillating at its natural frequency ν_0 is driven by a periodic force with frequency ν_f, it can become entrained by the external stimulus, thus oscillating at a frequency ν that is rationally related to the applied frequency ν_f.[1] Such frequency locking has been observed in various nonlinear systems of physical, chemical, and biological origin.[2−8]

Applied to distributed oscillatory reaction−diffusion systems, periodic forcing can lead to the formation of various complex spatiotemporal patterns. Most theoretical studies on resonant pattern formation in reaction−diffusion systems have concentrated on the forced complex Ginzburg−Landau equation (CGLE).[9,10] The forced CGLE represents a generic model of parametrically forced oscillatory reaction−diffusion systems valid near the soft onset of oscillations. When spatially homogeneous forcing with frequency $\nu_f \approx (n/m)\nu_0$ (where n and m are integers) is considered, typical resonant patterns in this equation consist of synchronized spatial domains with entrained oscillations that belong to either of n different phase states.[11] Different instabilities of the domain interfaces, where the oscillation phase is shifted from one phase domain to another, are possible in the various resonances.[12−18] Moreover, the presence of turbulence in the unforced system due to a diffusion-induced phase instability may lead to other interesting effects, including development of hexagonal structures[11] and spontaneous formation of cascades of phase kinks.[19]

Experimental studies[8,18,20−23] of resonant pattern formation in oscillatory reaction−diffusion systems have almost exclusively focused on the periodically forced, light-sensitive Belousov−Zhabotinsky (BZ) reaction. So far, all such experiments were performed in a nonchaotic parameter regime where stable rotating spiral waves are present in absence of forcing. The experiments revealed a wealth of spatiotemporal patterns developing under variation of the forcing parameters, including two-, three-, and four-phase clusters, irregular and localized clusters, stripes, and labyrinthine patterns.[8,18,20−23] In related works, the response of excitable[24−26] and subexcitable[27] BZ media to a periodic stimulus has also been studied.

* Corresponding author. E-mail: rotermun@fhi-berlin.mpg.de.

In this paper, the effects of periodic forcing on pattern formation are studied in a catalytic surface reaction, the oxidation of carbon monoxide on a platinum(110) single-crystal surface. In surface reactions, time-periodic, spatially uniform forcing can be easily implemented externally because global system parameters, such as temperature or partial pressures of the reactants in the gas phase, can be readily manipulated. In our study, the experimental parameters have been chosen in such a way that the unforced system exhibited chemical turbulence. In this way, in addition to ordered resonant patterns, different chaotic structures developing near the transition from resonant oscillations to turbulence could be observed.

Note that some effects of periodic forcing in CO oxidation on Pt(110) were already investigated shortly after self-sustained oscillations had been discovered in this reaction.[5] However, at that time, spatially resolved techniques for monitoring pattern formation were not yet developed and, thus, the observations were limited to purely temporal phenomena. A later study has investigated the role played by periodic forcing only with respect to the formation of standing waves.[28] The experiments presented in this paper show that also several other structures can be induced using this method.

The paper is organized as follows. The considered system and the experimental setup are introduced in the following section. In section 3, the results of our experimental investigations are presented. The properties of each type of forcing-induced pattern are described in detail. Resonant patterns are further characterized by means of a frequency demodulation technique[20] enabling the approximate reconstruction of amplitude and phase variables from the experimental data. The paper ends with a discussion of the obtained results in section 4.

2. Experimental Setup

The catalytic oxidation of CO on Pt(110) proceeds via the Langmuir−Hinshelwood mechanism;[29] i.e., molecules of oxygen and CO have to adsorb on the catalytic surface before the reaction to carbon dioxide can take place. Contrary to adsorption of CO, adsorption of oxygen is dissociative. An adsorbate-driven phase transition in the top surface layer[30] provides the mechanism for sustained temporal oscillations of the reaction rate. Spatial coupling across the surface due to diffusion of adsorbed

10.1021/jp0341927 CCC: $25.00 © 2003 American Chemical Society
Published on Web 07/25/2003

CO molecules gives rise to the formation of spatiotemporal patterns such as spiral waves, target patterns, and turbulence.[31]

In addition to the local diffusive coupling, global coupling through the gas phase is always present as a consequence of mass balance. Its effects have been previously investigated both experimentally[28,32] and theoretically.[33,34] To minimize the effects of internal gas phase coupling, specially prefabricated crystals with only small catalytically active areas have been used in the present study (see ref 35).

The experiments were carried out in an ultrahigh vacuum apparatus. Preceding each series of experiments, the sample was prepared by repeated cycles of Ar ion sputtering below 470 K and subsequent annealing to 750 K. An automated gas inlet system allowed controlled dosing of the reactants. Only purified gases (CO 4.7, O_2 5.6, and Ar 5.0) have been used. The system was operated as a continuous flow reactor by constant supply and pumping of gases.

To monitor pattern formation on the catalytic surface, we have employed photoemission electron microscopy (PEEM).[36] This technique produces real-time images of the lateral distribution of adsorbed species on the catalytic surface by displaying the local work function across a surface area of about 500 μm in diameter. While a monolayer of adsorbed oxygen atoms increases the work function by $\Delta\phi \approx 0.8$ eV, adsorbed CO molecules have a significantly weaker effect ($\Delta\phi \approx 0.3$ eV). As a result, surface areas mainly covered by CO are characterized by a higher PEEM intensity in the recorded two-dimensional images than regions predominantly covered by oxygen. The spatial resolution of images in our recordings was about 1 μm and the temporal resolution was 25 CCD camera frames per second.

Spatially uniform periodic forcing was implemented via the gas phase by using a frequency generator to control the dosing rate of CO gas. In this way, the CO partial pressure in the reaction chamber could be periodically modulated with a nearly harmonic signal of amplitude γ and frequency ν_f, while its temporal average p_0 was kept constant. The effects of forcing were investigated in a frequency range of 0.20 Hz $\leq \nu_f \leq$ 0.67 Hz. More rapid modulations of CO pressure in the reaction chamber were not possible at typical forcing amplitudes due to the finite pumping rate and limitations of the automated dosing system of CO gas. During the experiments, the effective CO partial pressure was measured with a differentially pumped quadrupole mass spectrometer.

3. Results

The conditions of temperature, oxygen partial pressure, and CO base pressure in the experiments were chosen such that the reaction was oscillatory, and moreover, uniform oscillations were unstable in the unforced system and spiral-wave turbulence spontaneously developed. This state is characterized by the creation of multiple rotating spiral waves that repeatedly undergo breakups, leading to a complex pattern of chemical turbulence with only short-range spatial correlations. A broad band of frequencies is then excited in the time series of local oscillations, so that the system does not possess a well-defined eigenfrequency. The initial reaction state was similar to that in previous experiments with global delayed feedback,[37] where the forcing signal was not fixed a priori but was made dependent on real-time properties of the developing patterns.

Periodic forcing was applied after spiral-wave turbulence had fully developed in the system. In such experiments, a rather large relative variation of CO partial pressure (about 10−20%, depending on temperature and base partial pressures) was necessary to suppress turbulence and to observe frequency locked patterns. In this range of the forcing amplitude, harmonic entrainment, where local oscillations at all resolving pixels in a pattern synchronized and locked to the forcing frequency, prevailed in the explored frequency range. However, at forcing frequencies $\nu_f \geq 0.5$ Hz, also frequency locked patterns with underlying 2:1 subharmonic entrainment have been observed.

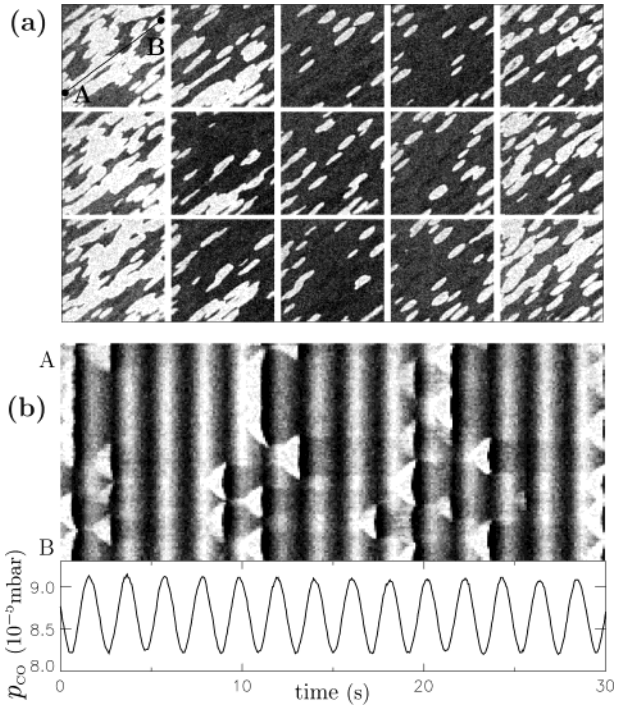

Figure 1. Intermittent turbulence under periodic forcing. (a) Displayed are fifteen subsequent snapshots of PEEM images of size 330 × 330 μm^2 (from left to right and top to bottom). Dark areas in the images are predominantly covered by oxygen, and bright regions are mainly CO covered. The time interval between subsequent images corresponds to the period of the driving force. (b) Space−time diagram displaying the temporal evolution of the pattern along the line *AB* indicated in the first image in (a). For comparison, the curve at the bottom shows the periodically varying signal of CO partial pressure in the reaction chamber. The forcing frequency is $\nu_f = 0.48$ Hz and the forcing amplitude is $\gamma = 10.3\%$ of relative CO partial pressure variation. The parameter values of temperature, oxygen partial pressure, and CO partial pressure are, respectively, $T = 513$ K, $p_{O_2} = 40.0 \times 10^{-5}$ mbar, and $p_0 = 8.7 \times 10^{-5}$ mbar.

In addition, by fixing the forcing amplitude below the transition to frequency locked uniform oscillations, also different types of nonresonant spatiotemporal patterns could be induced. In a wide range of forcing parameters, upon stepwise increase of the forcing amplitude, turbulent spiral waves were first replaced by intermittent turbulence before the transition to uniform oscillations occurred.

The observed state of intermittent turbulence is characterized by the repeated emergence and disappearance of localized turbulent bubbles on a background of locked uniform oscillations. In Figure 1a, a series of PEEM images is displayed, showing snapshots of intermittent turbulence at a given instant of subsequent forcing cycles. The repeated emergence of localized bubbles is rigidly correlated with the forcing period. The space−time diagram displayed in Figure 1b shows the pattern evolution along a cross section through the two-dimensional images. The localized bubbles are seen in the space−time diagram as bright triangular-shaped objects.

During several forcing periods, the bubbles reproduce until many of them are found, and then massive annihilation occurs

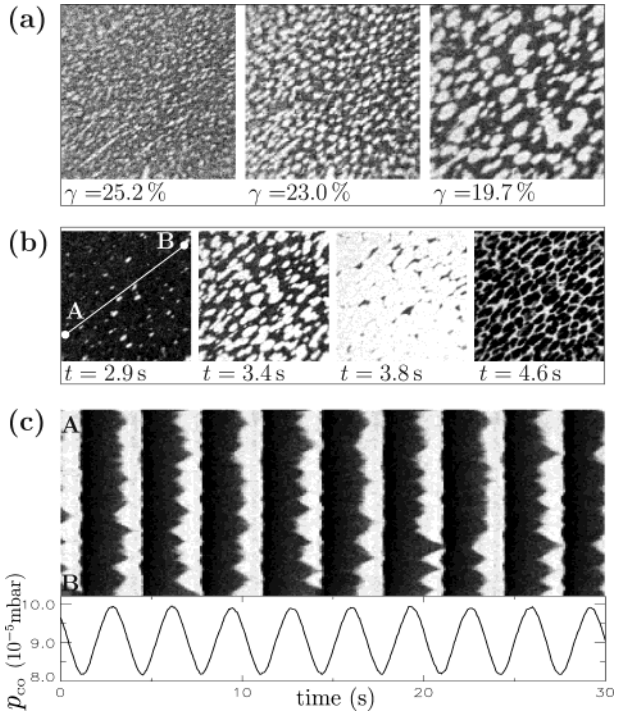

Figure 2. Cellular structures under periodic forcing. (a) Snapshots of PEEM images for three different values of the forcing amplitude. Each image is 330 × 330 μm^2 in size. The forcing frequency is fixed, ν_f = 0.30 Hz. (b) Four subsequent snapshots for γ =19.7%, sampled during a single forcing cycle. (c) Space−time diagram showing the pattern evolution along the line *AB* indicated in the first image in (b), and the corresponding temporal variation of CO partial pressure in the reaction chamber. The reaction parameters are T = 533 K, p_{O_2} = 40.0 × 10^{-5} mbar, and p_0 = 9.0 × 10^{-5} mbar.

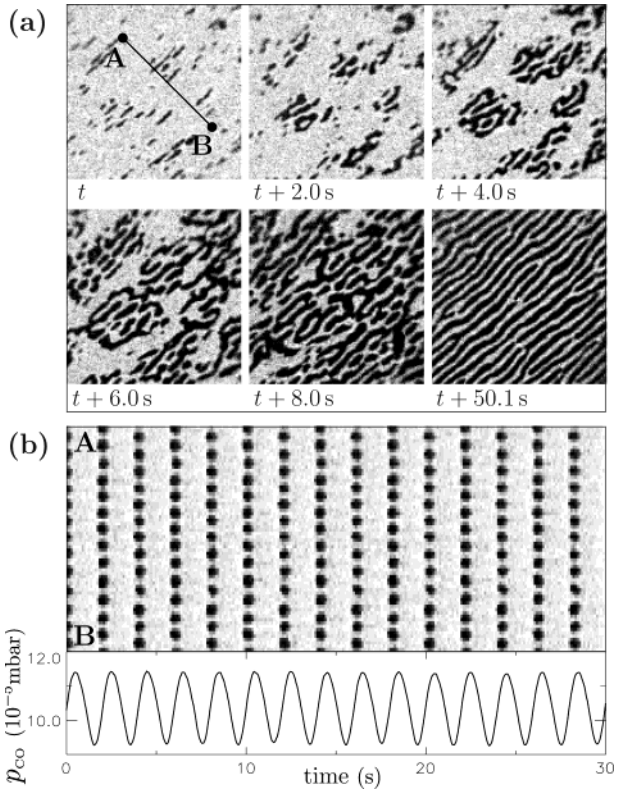

Figure 3. Irregular oscillatory stripes under periodic forcing. (a) Displayed are six snapshots of PEEM images of size 240 × 240 μm^2. The first five images illustrate the initial development of the pattern at time intervals of one forcing period between subsequent frames. The sixth image shows a later snapshot of the fully developed structure. (b) Space−time diagram for the fully developed pattern of irregular oscillatory stripes, taken along the line *AB* indicated in the first image in (a). The curve below shows the corresponding temporal variation of CO partial pressure. The forcing amplitude is γ = 20.2% and the forcing frequency is ν_f = 0.50 Hz. The reaction parameters are T = 531 K, p_{O_2} = 40.0 × 10^{-5} mbar, and p_0 = 10.4 × 10^{-5} mbar.

and only a few of them survive. In the shown example, such a cycle of pattern evolution, after which the density of bubbles is approximately repeated, takes five forcing periods. To see this, compare the images in the different rows of Figure 1a. However, the exact positions of bubbles are not repeated, and some of them disappear or are newly created from one such cycle to another, so that the long-term evolution of the pattern is chaotic. A similar state of intermittent turbulence has been observed also under global delayed feedback;[37] note that in this case, however, the forcing signal was not periodic.

Another type of nonresonant spatiotemporal pattern that was frequently observed in our experiments with periodic forcing is represented by oscillatory cellular structures. Upon a decrease of the forcing amplitude, such arrays of cells arise as small modulations of frequency locked uniform oscillations. Typical PEEM images of cell arrays taken at different values of the forcing amplitude are displayed in Figure 2a. While at higher forcing amplitudes, the cells are small and visible only during a short time interval of each oscillation cycle, the size of individual cells significantly grows upon a further decrease of γ. The cells then become more pronounced, so that they are visible for larger fractions of each forcing cycle. Starting from resonant uniform oscillations, the formation of cellular structures has also been observed upon an increase of the forcing frequency.

The temporal evolution of a typical example of a developed, disordered array of cells at fixed forcing parameters is illustrated in Figure 2b,c. The four PEEM images displayed in Figure 2b are sampled within a single forcing cycle. In the first frame, the cells emerge as small CO covered islands whereas the main part of the surface is predominantly covered by oxygen. The bright regions then extend (second frame), until they fill almost the entire imaged surface area (third frame). The cell array is again seen for a short instant during the transition back to the mainly oxygen covered state (fourth frame). From one forcing cycle to another, however, the cell positions change significantly, so that the cells form a complex, irregular pattern in the space−time diagram taken along a cross-section through the two-dimensional images; see Figure 2c.

At higher forcing frequencies, $\nu_f \geq 0.5$ Hz, additional resonant patterns arise due to 2:1 subharmonic entrainment of local oscillations. At the low-frequency edge of this resonance, irregular oscillatory stripes prevail. The sequence of PEEM images displayed in Figure 3a illustrates the growth mechanism of such a structure. The pattern originates from small-amplitude uniform oscillations taking place around a mainly CO covered state. The predominantly oxygen covered state is only reached at certain locations on the surface where fragments of stripes first appear. During the further evolution, starting from such locations the structure grows stripe by stripe, until it occupies the entire imaged surface area. As time goes on, the number of dislocations in the pattern, i.e., the regions where individual stripes merge to form a forklike structure, slowly decrease and a more regular, quasi-stationary configuration is established; see the sixth frame in Figure 3a. Due to diffusion anisotropy of the Pt(110) single crystal surface, the stripes are then mainly oriented along the surface direction of fast CO diffusion (the [1$\bar{1}$0] direction).

Figure 3b displays a space−time diagram of the fully developed stripe pattern taken along a cross-section perpendicular to the orientation of stripes. The dark stripes are seen in this diagram only during relatively short intervals of each oscillation cycle. After each forcing period, the locations of the stripes are shifted, and new stripes have appeared in the middle between those seen at the previous cycle. Thus, the initial pattern is repeated every two forcing cycles. Local oscillations within the central regions of alternating stripes hence have the same shape and frequency ($\nu = \nu_f/2$), but are shifted in time by one forcing period.

To further analyze the dynamics of oscillatory stripes, a frequency demodulation technique[20] useful for the characterization of resonant patterns has been employed. To determine the temporal response of each resolving pixel (x, y) of the pattern, the Fourier transform of the time series at each pixel was calculated. The average power spectrum over all pixels showed two distinct peaks at the frequencies $\nu_f/2$ and ν_f. Higher order harmonics were also present.

To obtain separate information on the local oscillation magnitude and phase associated with the different excited temporal modes, the complex Fourier coefficients $a(x,y)$ that correspond to the modes with frequencies ν_f and $\nu_f/2$ were then extracted from the Fourier spectrum for each pixel. By plotting the spatial distributions of the quantities $\arg(a)$ and $|a|$, phase and amplitude images were obtained for the two frequencies. These are displayed in Figure 4a,b, respectively, where the plots in the left column show the response of the system at frequency ν_f, and the right column shows the results of a frequency demodulation at $\nu_f/2$. In Figure 4c, for both frequencies the complex Fourier coefficients a at each pixel are plotted into the complex plane. Each point in the resulting phase portraits corresponds to a pixel in the original pattern. Finally, Figure 4d displays histograms of the distribution of phase angles in the abscissa range $[-\pi,\pi]$.

Examining Figure 4, one finds that the spatial pattern associated with the mode ν_f is almost uniform. Spatial variations are observed only as small depressions of the amplitude field at some positions where different stripes merge. In contrast, the array of stripes is clearly seen in the patterns associated with the mode $\nu_f/2$. The corresponding phase image shows an array of bright and dark stripes that are of opposite phase. In the amplitude pattern, it is seen that the oscillation magnitude in the mode $\nu_f/2$ is greatly reduced along the boundaries between the π-shifted stripes. In the corresponding phase portrait, the pixels are spread along a straight line that crosses the origin of the complex plane, indicating that the oscillation magnitude actually vanishes along the lines that separate adjacent π-shifted stripes. The two phase states are evenly weighted within the pattern, as can be seen in the phase histogram. Thus, by means of frequency demodulation, it is found that, though significant power is present in the harmonic mode, the spatial information of the stripes is solely contained in the 2:1 subharmonic mode and the pattern consists of two phase-locked, π-shifted phase states.

At still higher forcing frequencies than needed for the observation of oscillatory stripes, cluster patterns are induced by the periodic stimulus at moderate forcing amplitudes. Upon the formation of phase clusters, the surface splits into relatively large domains belonging to one of two different dynamical states; see the top row of Figure 5a showing three snapshots of PEEM images at time intervals of one forcing period between subsequent frames. After each period of the driving force, predominantly oxygen and CO covered regions have interchanged with respect to the previous PEEM image, so that the pattern almost exactly repeats after two forcing cycles. Thus, the local oscillations within the different domains are also entrained at half the frequency of the driving force and oscillate in anti-phase, as for oscillatory stripes. However, an intrinsic wavelength is absent in the case of phase clusters. Both cluster patterns and oscillatory stripes transform into resonant uniform oscillations upon a sufficiently strong increase of the forcing amplitude.

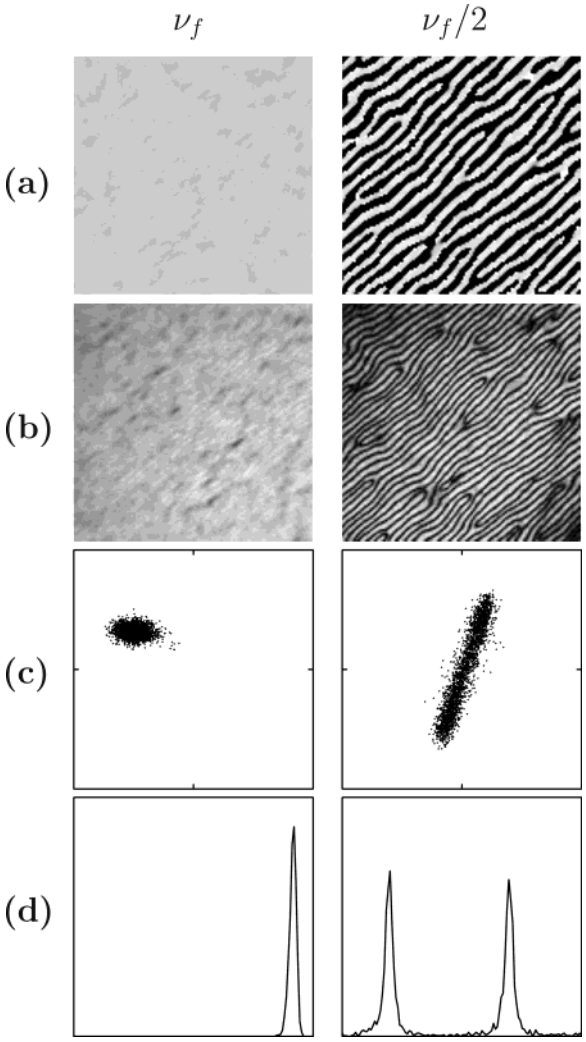

Figure 4. (a) Phase patterns, (b) amplitude patterns, (c) phase portraits, and (d) phase histograms of a pattern of irregular stripes demodulated at the frequencies ν_f (left column) and $\nu_f/2$ (right column). In the phase and amplitude patterns, dark regions corresponds to low values of the shown quantities. The phase portraits show each of the Fourier coefficients a plotted into the complex plane, where the abscissa is $\mathrm{Re}(a)$ and the ordinate is $\mathrm{Im}(a)$. The oscillation magnitude $|a|$ for each point corresponds to its distance from the origin of the complex plane, and the phase $\arg(a)$ is given by the polar angle. The phase histograms display the distributions of phases $\arg(a)$; the abscissa range is $[-\pi,\pi]$ and the ordinate units are arbitrary.

The temporal evolution of phase clusters in our experiments is illustrated in Figure 5b. Examining the space−time diagram, one finds that the interfaces between domains of opposite phase are stationary and that the spatial distribution of domains is stable over several forcing periods. Sometimes, however, it was observed that phase clusters underwent a sudden rearrangement after which a new spatial configuration of domains was established, which again was stable for a certain number of forcing periods.

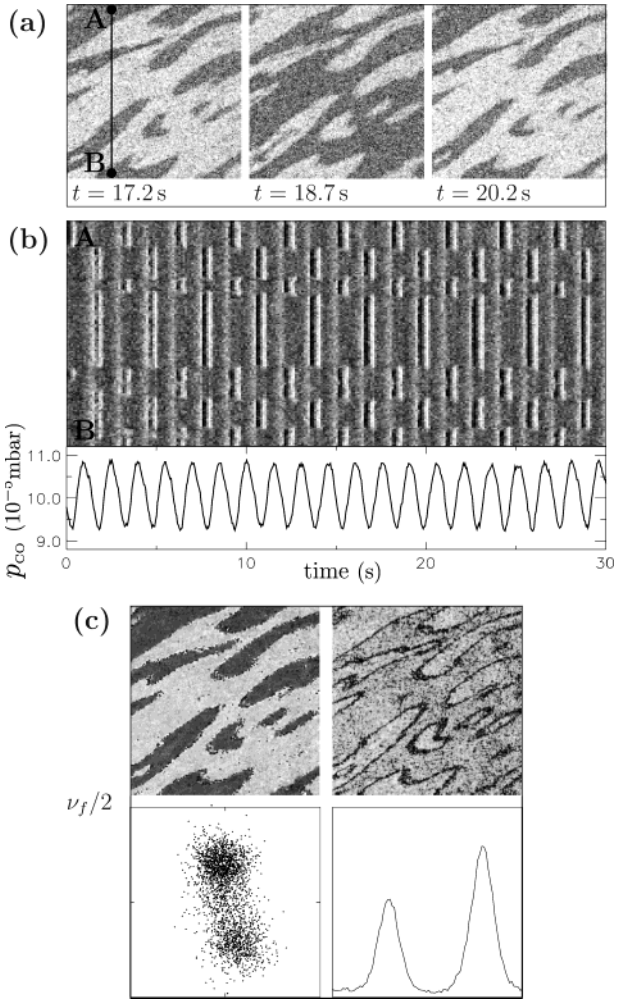

Figure 5. Phase clusters under periodic forcing. (a) Three snapshots of PEEM images of size 300×300 μm^2, separated by time intervals of one forcing period between subsequent images. (b) Space−time diagram taken along the line *AB* indicated in the first image in (a), and the corresponding temporal variation of CO partial pressure. (c) Phase pattern (top left), amplitude pattern (top right), phase portrait (bottom left), and phase histogram (bottom right) for the phase clusters demodulated at the frequency $\nu_f/2$. The forcing parameters are $\gamma = 16.4\%$ and $\nu_f = 0.67$ Hz, and the reaction parameters are $T = 523$ K, $p_{O_2} = 40.0 \times 10^{-5}$ mbar, and $p_0 = 10.1 \times 10^{-5}$ mbar.

For further analysis of the pattern of phase clusters presented in Figure 5a,b, we again make use of the above-described frequency demodulation technique. The result of a demodulation at the subharmonic mode with frequency $\nu_f/2$, using data from a stable period of the pattern, is displayed in Figure 5c. From left to right and top to bottom, the frames show the resulting phase pattern, amplitude pattern, phase portrait, and histogram of phases. Note that the oscillation amplitude is strongly reduced in the domain interfaces (black lines in the top right frame in Figure 5c), and that it is the same within the domains of opposite phase. The phase portrait shows two spots of accumulating points, corresponding to the pixels located within the anti-phase domains; the scattering of points is due to experimental noise. The points that connect these spots correspond to pixels located within the phase fronts. As seen in the phase histogram, the two phase states are not evenly weighted. The size ratio between the two peaks was different each time phase clusters were observed in our experiments. Note that such behavior was not observed for phase clusters induced by global delayed feedback,[37] where phase balance of the domains was usually present.

4. Discussion

In this paper, we have studied the effects of periodic external forcing on chemical turbulence in CO oxidation on Pt(110). Using this method, spiral-wave turbulence could be replaced by various chaotic and resonant spatiotemporal structures. Below, the observed structures are discussed with respect to experimental and theoretical results obtained in previous studies of the light-sensitive Belousov−Zhabotinsky (BZ) reaction and the forced complex Ginzburg−Landau equation (CGLE).

In our work, two different types of nonresonant patterns have been investigated in the vicinity of harmonic entrainment. Intermittent turbulence under periodic forcing is characterized by the repeated emergence of localized turbulent bubbles on the background of uniform oscillations. In the forced CGLE, intermittent turbulence has been extensively studied in one space dimension.[19] It is characterized by turbulent cascades of kink breeding on a background of uniform or phase-turbulent oscillations. Detailed studies of intermittent turbulence in the forced CGLE in two space dimensions are still lacking.

Disordered cellular structures in our experiments represent another type of pattern forming due to competition of the synchronizing effect of forcing and the destabilizing effect of diffusion. Numerical simulations of the forced amplitude equation, performed under conditions of phase instability in absence of forcing, have shown a transition from uniform oscillations to small-amplitude hexagonal cells, whose symmetry was then destroyed by further instabilities,[11] resulting in phase turbulence. Such instabilities may also explain the spatial disorder of forced cells observed in the present study. However, the arrangement of cells may be also affected by localized structural defects always present on the single crystal surface. So far, neither intermittent turbulence nor cellular structures have been reported in the periodically forced BZ reaction, possibly because turbulence in the unforced system was absent in such experiments.

Irregular oscillatory stripes consist of two phase-locked, π-shifted states and are due to 2:1 subharmonic entrainment of local oscillations. In our experiments, they grow via nucleation of stripes at various locations on the surface. A similar growth mechanism was recently described in the framework of the forced CGLE, where it led to the development of a pattern of irregular stripes forming a labyrinthine structure.[18] Standing-wave labyrinthine patterns due to this mechanism were also reported in the light-sensitive BZ reaction.[18] The lack of a clearly visible labyrinthine structure in our experiments might be explained by the diffusion anisotropy on the Pt(110) single-crystal surface, which favors the orientation of stripes in [110] direction. A stretched, large-scale labyrinth-like structure was probably present but could not be identified within the relatively small imaged surface area. However, the phase and amplitude properties of the observed oscillatory stripes are strikingly similar to those of the labyrinths in the forced BZ reaction and the forced CGLE.[18]

Two-phase clusters represent another subharmonic entrained pattern predicted by the forced CGLE[11,12] and observed in the forced BZ reaction.[20,22] From analysis of the forced CGLE,[12] within stationary domain interfaces of two-phase clusters one expects a nodal line where the oscillation amplitude vanishes and the phase undergoes a jump of π. The reconstruction of amplitude and phase data enabled us to identify such front properties also in our experiments. Although not observed in the present study, we note that phase clusters with different front properties and also further types of patterns may exist in the CO oxidation system at forcing frequencies larger than ν_f

= 0.67 Hz, a region in parameter space that was not accessible due to limitations of the gas dosing system.

In conclusion, by means of periodic external forcing, a variety of spatiotemporal patterns could be induced in experiments with CO oxidation on Pt(110). Although the system was not operated close to a Hopf bifurcation and oscillations were not harmonic, many of our observations are qualitatively well described by the forced complex Ginzburg−Landau equation. Our observations describe the self-organized behavior of a periodically forced oscillatory reaction−diffusion system in a dynamically rich parameter range where the unforced system exhibits chemical turbulence.

Acknowledgment. Financial support of the Deutsche Forschungsgemeinschaft in the framework of SFB 555 "Complex Nonlinear Processes" is gratefully acknowledged. We thank A. S. Mikhailov for helpful discussions.

References and Notes

(1) Thompson, J. M. T.; Stewart, H. B. *Nonlinear Dynamics and Chaos*; Wiley: Chichester, U.K., 1986.
(2) Buck, J.; Buck, E. *Sci. Am.* **1976**, *234*, 74.
(3) Guevara, M. R.; Glass, L. *J. Math. Biol.* **1982**, *14*, 1.
(4) Bohr, T.; Bak, P.; Jensen, M. H. *Phys. Rev. A* **1984**, *30*, 1970.
(5) Eiswirth, M.; Ertl, G. *Phys. Rev. Lett.* **1988**, *60*, 1526.
(6) Pivka, L.; Zheleznyak, A. L.; Chua, L. O. *Int. J. Bif. Chaos* **1994**, *4*, 1743.
(7) Niedernostheide, F.-J.; Brillert, C.; Kukuk, B.; Purwins, H.-G.; Schulze, H.-J. *Phys. Rev. B* **1996**, *54*, 14012.
(8) Petrov, V.; Ouyang, Q.; Swinney, H. L. *Nature* **1997**, *388*, 655.
(9) Gambaudo, J. M. *J. Diff. Eq.* **1985**, *57*, 172.
(10) Elphick, C.; Iooss, G.; Tirapegui, E. *Phys. Lett. A* **1987**, *120*, 459.
(11) Coullet, P.; Emilsson, K. *Physica D* **1992**, *61*, 119.
(12) Coullet, P.; Lega, J.; Houchmanzadeh, B.; Lajzerowicz, J. *Phys. Rev. Lett.* **1990**, *65*, 1352.
(13) Mizuguchi, T.; Sasa, S. *Prog. Theor. Phys.* **1993**, *89*, 599.
(14) Elphick, C.; Hagberg, A.; Meron, E. *Phys. Rev. Lett.* **1998**, *80*, 5007.
(15) Elphick, C.; Hagberg, A.; Meron, E. *Phys. Rev. E* **1999**, *59*, 5285.
(16) Hemming, C.; Kapral, R. *Faraday Discuss.* **2001**, *120*, 371.
(17) Hemming, C.; Kapral, R. *Physica D* **2002**, *168*, 10.
(18) Yochelis, A.; Hagberg, A.; Meron, E.; Lin, A. L.; Swinney, H. L. *SIAM J. Appl. Dyn. Syst.* **2002**, *1*, 236.
(19) Chaté, H.; Pikovsky, A.; Rudzick, O. *Physica D* **1999**, *131*, 17.
(20) Lin, A. L.; Bertram, M.; Martinez, K.; Swinney, H. L.; Ardelea, A.; Carey, G. F. *Phys. Rev. Lett.* **2000**, *84*, 4240.
(21) Lin, A. L.; Hagberg, A.; Ardelea, A.; Bertram, M.; Swinney, H. L.; Meron, E. *Phys. Rev. E* **2000**, *62*, 3790.
(22) Vanag, V. K.; Zhabotinsky, A. M.; Epstein, I. R. *Phys. Rev. Lett.* **2001**, *86*, 552.
(23) Martinez, K.; Lin, A. L.; Kharrazian, R.; Sailer, X.; Swinney, H. L. *Physica D* **2002**, *168*, 1.
(24) Steinbock, O.; Zykov, V.; Müller, S. C. *Nature* **1993**, *366*, 322.
(25) Braune, M.; Engel, H. *Chem. Phys. Lett.* **1993**, *211*, 534.
(26) Braune, M.; Schrader, A.; Engel, H. *Chem. Phys. Lett.* **1994**, *222*, 358.
(27) Sendiña-Nadal, I.; Mihaliuk, E.; Wang, J.; Pérez-Muñuzuri, V.; Showalter, K. *Phys. Rev. Lett.* **2001**, *86*, 1646.
(28) von Oertzen, A.; Rotermund, H. H.; Mikhailov, A. S.; Ertl, G. *J. Phys. Chem. B* **2000**, *104*, 3155.
(29) Engel, T.; Ertl, G. *Adv. Catal.* **1979**, *28*, 1.
(30) Gritsch, T.; Coulman, D.; Behm, R. J.; Ertl, G. *Phys. Rev. Lett.* **1989**, *63*, 1086.
(31) Jakubith, S.; Rotermund, H. H.; Engel, W.; von Oertzen, A.; Ertl, G. *Phys. Rev. Lett.* **1990**, *65*, 3013.
(32) Rose, K. C.; Battogtokh, D.; Mikhailov, A.; Imbihl, R.; Engel, W.; Bradshaw, A. M. *Phys. Rev. Lett.* **1996**, *76*, 3582.
(33) Falcke, M.; Engel, H. *J. Chem. Phys.* **1994**, *101*, 6255.
(34) Falcke, M.; Engel, H.; Neufeld, M. *Phys. Rev. E* **1995**, *52*, 763.
(35) Pollmann, M.; Bertram, M.; Rotermund, H. H. *Chem. Phys. Lett.* **2001**, *346*, 123.
(36) Rotermund, H. H. *Surf. Sci. Rep.* **1997**, *29*, 265.
(37) Kim, M.; Bertram, M.; Pollmann, M.; von Oertzen, A.; Mikhailov, A. S.; Rotermund, H. H.; Ertl, G. *Science* **2001**, *292*, 1357.